An Exploration into Modelling the Relationship Between Structural and Functional Connectomes

Samuel Finestone

1 Introduction

Understanding how the brain functions has been an area of intense study over the past several years. Although the brain has been looked at through different granularity lenses, we will be exploring the more practical lens, the connectome. Due to the brain's sensitive and very complex nature, mapping the connectome to a very detailed level has been a laborious task. The connectome is the constitutes of the various pathways of interconnections of cells, regions in the brain or nervous system. These bundles of pathways are made up of axons, connecting these different parts of the brain. These patterns can be broken down into structural and functional connectivity [1]. Where structural connectivity refers to the axon fibre bundles that physically link the different regions, whereas the functional connectivity deals with the interdependence in time segments of neural activity in cortical regions or cell populations [1]. Either notion use different sub-modalities of magnetic resonance imaging (MRI) to extract valuable information to understand how the brain functions. In this project my team and I attempt to use these different MRI scans to model the relationship between these structural and functional connectivity maps.

2 Core Task 1: Graph properties of structural and functional connectomes

To build an understanding of the full structural connectivity map there are a few steps required to obtain a detailed graphical representation of the brain's structure. Researchers typically use high resolution structural MRI images and then subsequently parecelate the cortex into anatomically sub-regions. Then, tractography is carried out throughout the brain, and the edges between each pair of regions is assembled into an abstract graph [1]. In this project we are provided with a set of multi-modal imaging data from a single healthy adult coupled with a series of structural connectomes derived using several different anisotropy thresholds. Since a lot of the pre-processing of the MRI imaging was done by the TractoR software package [1]. The most important files used to reconstruct a structural connectome are listed below.

- structural/refT1.nii.gz: T1-weighted structural image
- structural/parcellation.nii.gz: A cortical parcellation, where each voxel is labelled with a cortical region (int)
- structural/parcellation.lut: A table of information about the labelled regions in the parcella-

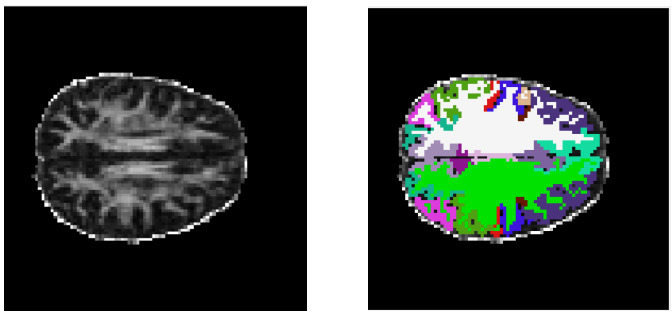

(a) The dMRI data

(b) dMRI overlayed with the parcelated brain regions

Figure 1: The 40th slice of the dmri data overlayed with its labeled brain regions

tion

- diffusion/data.nii.gz: The dMRI dataset, a 4D volume with gradient direction varying along the fourth dimension
- diffusion/dti_FA.nii.gz: A map of fractional anisotropy
- diffusion/parcellation.nii.gz: The same parcellation as above but translated for the diffusion data
- functional/data.nii.gz: The rs-fMRI dataset, a 4D volume with time varying along the fourth dimension to align the individual volumes and apply temporal filtering
- functional/parcellation.nii.gz: The same parcellation as above, converted for the functional data

To help understand the provided data as well as the data needed to construct the structural connectome, the cortical parcelation data were overlayed onto the base diffusion MRI data. Provided by the files *functional/data.nii.gz* as the base layer and the *diffusion/dti_FA.nii.gz* as the overlay. An example of the underlay and overlay of representation are displayed in Figure 1. Where the overlay displays a specific color for each coherent cortical region in the FA map. Although this Figure 1(b) contains a few colors, there are a total of 108 labelled regions throughout this dataset. The file *structural/parcellation.lut* contains the table for each color to labelled cortical region.

FA maps can be used to quantify the white matter (WM) integrity in the brain. Hence, we can use these properties to threshold FA maps at different values, allowing for the exclusion of specific regions of the brain for data processing. We look at taking an array of thresholds of the functional anisotropy (FA) map at differing values, from 0.1 to 0.8 in increments of 0.1. Thereby creating a means to identify well-defined pathways. This was done by allowing the sub-threshold voxel values to be equal to zero. As demonstrated in Figure 2, as the threshold increases the pixels with lower FA values are excluded while the remaining pixels represent regions in the brain with the highest WM integrity. Specifically the higher WM integrity lies within the surrounding area of the brain, indicating that those areas exhibit large number of structured pathways [2]. Additionally, as the threshold increases the less the number of voxels tend to be converted to zero, suggesting that there are fewer higher value gradients in a dMRI than lower ones as illustrated in Figure 2(b).

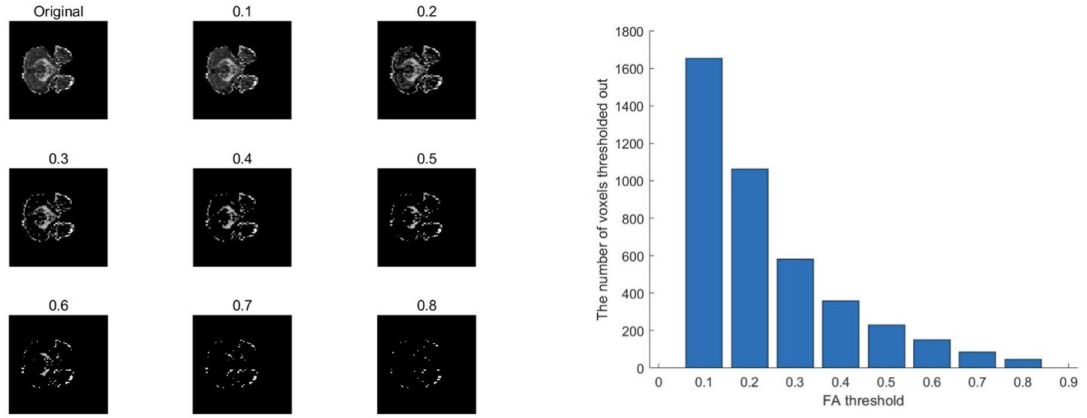

(a) Applying different thresholds to the original FA map (slice 30)

(b) Distribution of the remaining voxels after the filtering of each threshold

Figure 2: Changing the FA threshold

Next explored the structural connectomes after applying the different FA thresholds by evaluating multiple graph properties such as edge density, mean shortest path, efficiency and mean clustering coefficient. Understanding the sparsity of these graphs can be indicative of fewer connections between cortical regions. The cluster coefficient is equivalent to the fraction of the nodes neighbours that are also linked to each other, and the mean clustering coefficient reflects the proportion of clusters connectivity around individual nodes. The 8 FA graphs were provided along with the previous files. For each FA graph the 4 different properties were evaluated using the Brain Connectivity Toolbox (BCT) package. The results of the edge sparsity property is displayed in Figure 3(b). Which shows a decreasing linear relationship between the thresholds and the edge density in the graphs. Additionally, as the FA threshold increases the mean clustering coefficient decreases since more nodes are being excluded. The two spikes in the plot occur because the mean clustering coefficient is normalized individually for each node and can therefore be disproportionately affected by nodes with a lower number of neighbours. The mean shortest path length is the average shortest path length between all pairs of nodes in a network. For this experiment if we look at Figure 3(a), as the FA threshold increases the more sub-threshold voxels are excluded from the graph, causing the path lengths between brain regions to become longer. It is important to note that from 0.6 to 0.7 there is no greater impact on the metric since it is likely that the portion of the remaining nodes are disconnected from each other. Whereas, if we increase the threshold from 0.7 to 0.8 reduces the mean shortest path, this occurs because the now the model is removing some of this disconnected nodes from the graph. Finally, the efficiency metric is defined as the average inverse shortest path length. Hence, as the FA threshold increases the larger the efficiency since more nodes are going to be disconnected from each other.

Functional representation of the connectome is constructed differently, it requires recording different cortical regions or even voxel level regions activity over a period of time. Then using time series methods, for instance cross-correlation from resting state fMRI (re-fMRI), we construct a correlation matrix or a matrix of statistic dependency among time courses [1]. That is typically a

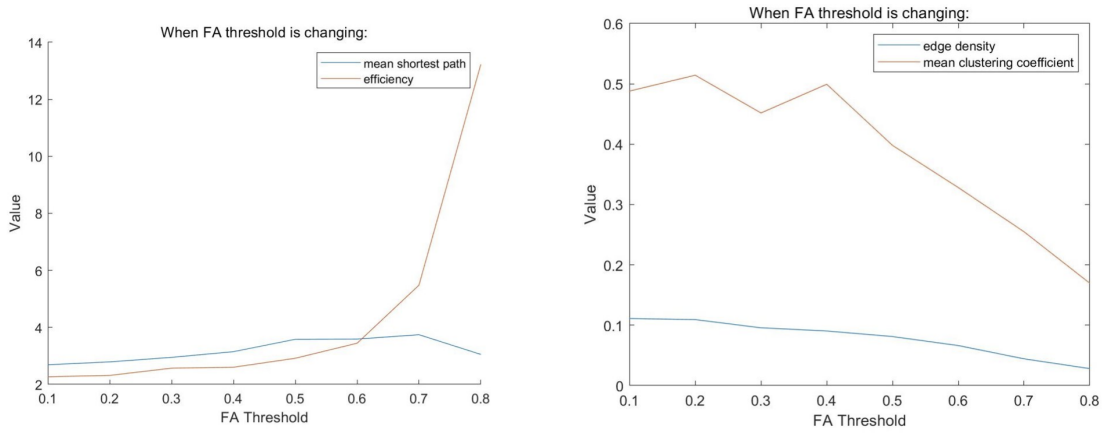

(a) Mean shortest path and efficiency against FA thresholds

(b) Edge density and mean clustering coefficient against FA thresholds

Figure 3: Plotting the 4 different graph metrics

full matrix, not sparse, every element in that matrix has a non-zero entry to it and can be positive or negative. We look at computing a weighted functional connectome, by firstly extracting an average time series in each cortical region and then deriving a correlation matrix using the shrinkage approach. In the case of fMRI, the functional connectivity is a correlation matrix, where many edges are interdependent, which means we cannot construct null models the way you can do with a wiring diagram. This process was implemented by using the files *functional/data.nii.gz*, *functional/parcellation.nii.gz* and the information table *functional/parcellation.lut*. Once the average times series of each cortical region is extracted, from the files, we use the we used the *corshrink()* function to derive a correlation matrix. This function also takes as parameter not only average time series data but a shrinkage parameter, λ. For this task, we selected a range of different lambda values, 0.1 to 0.8 in steps of 0.1. The resulting matrix was then filtered by giving correlations entries that less than 0.1 to be 0, otherwise 1. Then the graph metrics were recomputed using BCT, the results are represented in Figure 4. As the λ increases the edge density has an exponential decay relationship, which we would expect as the less significant nodes in the graph with respect to target nodes are being discarded. The mean clustering coefficient decreases very slightly and then increases from 0.7 to 0.8, this is happens since the metric is disproportional influenced by functional connections with a lower number of neighbouring nodes. The mean shortest path and efficiency both exhibit an exponential relationship with the shrinkage parameter. As less significant functional connections in the correlation matrix are being removed, the further the neural activity is happening from each pair of functional connections. Subsequently, we consider the effects of retaining or discarding negative correlations with absolute values greater than 0.1. Both the retained and discarding the sub-threshold values are displayed in the Figure 5, for easier understanding. Overall, if we are to apply this filtering of an absolute value, we see that the opposite trend is exhibited. Indicating that the positive correlations between regions tend be closer in proximity and the graphs tend to be more dense as the λ increases, since the edge density increases as well as the mean clustering coefficient. Finally, the efficiency is inversely proportionate to the mean shortest path, hence why we do see that it tends to decrease over λ.

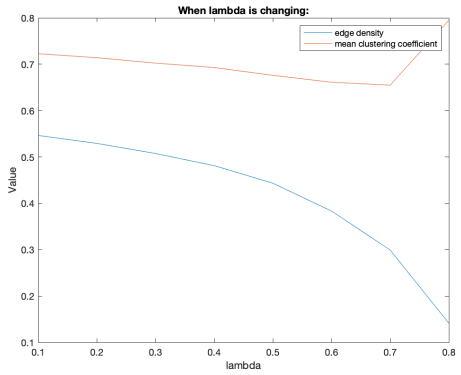

(a) Mean shortest path and efficiency against λ

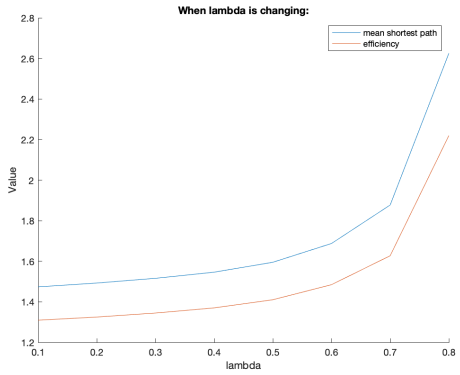

(b) Edge density and mean clustering coefficient against λ

Figure 4: Plotting the 4 different graph metrics when changing λ

It is important to specify that in the functional connectivity graph is built of nodes that are mean average time series data of a region of the brain and the edges weight are represent correlation coefficient of two time series of two nodes [3]. Hence, when we are discarding a negative edge weight with absolute value greater than 0.1 then we are dealing with pair of regions that have significantly less influence on each others neural activity. Whereas, if we retain them then we keep the pairs of regions that both affect and disproportionately affect their neural activity. However, it must be interesting to note that the functional connectivity graph will change with age and gender. As with time, structural nodes decay and therefore affecting the overall functional connectivity in the brain. Whereas with men and women have different brain region sizes which would affect both functional and structural graphs [4].

3 Core Task 2: Modelling the relationships between connectomes

Next, we explore the relationship between structural and functional connectomes by using different linear models to predict functional connectivity weights, f_{ij} between the regions i and j from the structural connectivity weights, s_{ij}. Due to the sparse nature of the structural connectivity matrix, we also consider the indirect structural connectivity weights, t_{ij} which represents connection of between two regions going through exactly one other a middle region first. These connections were computed as follows, $t_{ij} = \max_k(\min(s_{ik}, s_{kj}))$, where $s_{ij}, s_{kj} \neq 0$. Each of the linear models include and exclude these indirect connections. The following models were fitted to the data in turn.

$$f_{ij} = \alpha_{ij} + \beta_{ij} s_{ij} \tag{3.1}$$

$$f_{ij} = \alpha_{ij} + \beta_{ij} s_{ij} + \gamma_{ij} s_{ij}^2 \tag{3.2}$$

$$f_{ij} = \alpha_{ij} + \beta_{ij} + t_{ij} \tag{3.3}$$

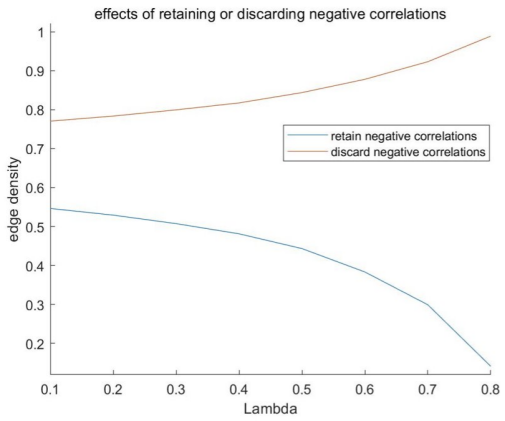

(a) Edge density againt λ

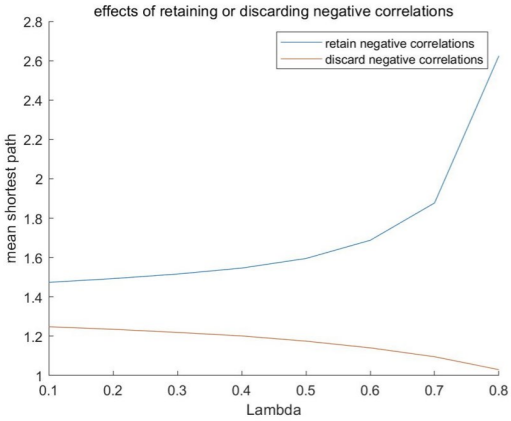

(b) Mean shortest path against λ

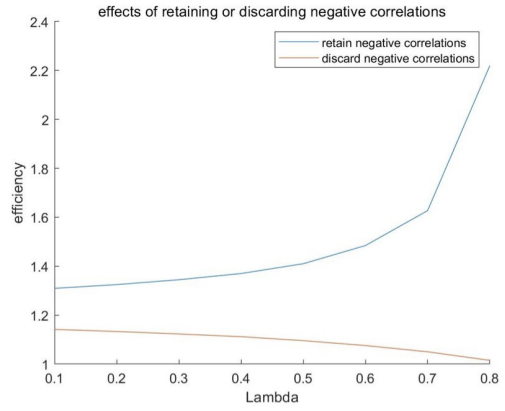

(c) efficiency against λ

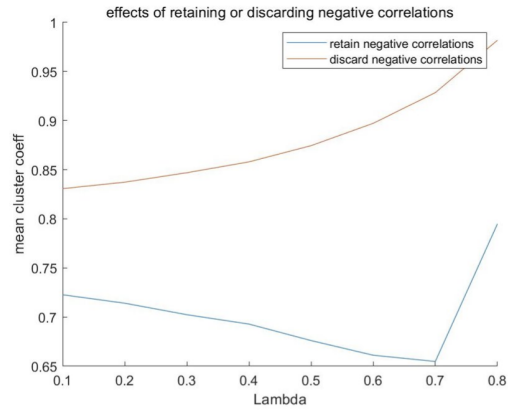

(d) Mean clustering coefficient against λ

Figure 5: Effects of retaining or discarding negative correlations with absolute value greater than 0.1

Model	SEE	AIC	BIC
Model 1	14.2715	-201.6323	-198.799
Model 2	22.915	-197.8198	-194.042
Model 3	14.6356	-198.9278	-196.0945
Model 4	15.7594	-194.4284	-190.6506
Model 5	15.5515	-196.6004	-192.8226

Table 1: Performance metrics for each linear model

$$f_{ij} = \alpha_{ij} + \beta_{ij} + t_{ij} + \gamma_{ij} t_{ij}^2 \tag{3.4}$$

$$f_{ij} = \alpha_{ij} + \beta_{ij} + t_{ij} + \gamma_{ij} t_{ij} \tag{3.5}$$

Each coefficient $\alpha, \beta and \gamma$ are estimated separately for each existing edge using a ordinary least square (OLS) approach. For each model the regression was performed on 19 adult data. The provided data was given as 19 separate resting state fMRI and weighted FA maps. To help compare the models and select the best performing one, we computed different performance metrics. For each of the 5 models we evaluated the sum of squared errors (SSE) using a leave one out cross validation. The Akaike and Bayesian Information Criterion (AIC and BIC) were also calculated, the results of these metrics are displayed in Table 1. Both criterions are used to score and select models. The AIC statistic penalizes the complexity in the models less than the BIC and places more importance on the model's performance on the training data, and thereby rewarding the more complex model. Hence, why model 4 has the lowest AIC score. Whereas the BIC, puts more emphasis on the complexity of the model, in other words the model with least complex relationship has the highest score. We see that Model 1 has the lowest SEE as well as the lowest AIC and BIC, therefore the better model overall.

We then considered analysing the quality of the model parameter estimates across the different edges. This analysis was done by computing the variance of a α_{ij} across the 19 folds and this by the maximum variance in the between all α_{ij}, the result was then built into a 68x68 matrix of variance intensities. This was done for the other parameters as well. The same approach was done for the residuals of the model. The results of the quality in model 1 can be seen in Figure 6, where each square matrix is a 68 by 68 representing the different normalized parameter variances. Where each element in the matrix represents the strength of that variance or in the case of the SEE the higher element intensity the higher the error. In the first row of Figure 6, we do see that the top left and bottom right corners of the matrix contain more shades of white, indicating that there tends to be more uncertainty in the parameters with edges that link regions of the brain that are closer from each other. Whereas the the top right and bottom left corners of the estimated parameters, the intensities are much darker, which indicates that there is a lot more certainty in the those values, consequently the SSE tend to be lower values. Furthermore, if we look at a closer up example of, the second row of Figure 6, the higher the variance in the parameters the higher the SSE and thus the worse the performance. Although this analysis was only done for the first model, the other models had similar representations with their estimated parameters.

Next, we repeated the previous task but instead we used a single set of coefficients for all edges. In other words for each fold we computed an OLS where the feature matrix X is very large, of dimension (68x68x18,2) and Y is of dimension (68x68x18,1) and the estimated parameters for every fold was a single value. The average SSE over the holdout sets for each fold was recorded, Table 2. This

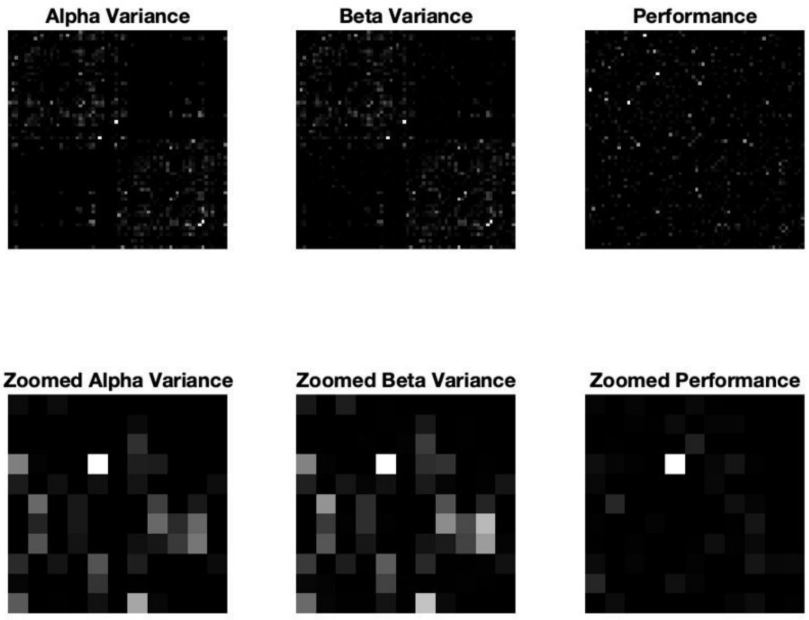

(a)

Figure 6: First row contains the parameter variances and SEE. The second row is a close up example of high intensity correlation across all three

method leads to much worse performance, since we are now trying to compute a single set of weights for all the values of f_{ij} and this just ends up with a very general weight. Additionally the predicted f_{ij} are very small values, close zeros, therefore the SSE values are simply the total sum of squares of the actual f_{ij} values. The quality of the parameters are also recorded this time computing the mean and variance of the parameters, these values are displayed in Table 3. It is noticeable to see that the estimated parameters means and variance are very small values, indicating that the models clearly are generalizing and do not vary much in their predicted f_{ij} values.

Based on the previous experiment using more than just a single value for the coefficients, Table 1, we find that the structural connectivity weight S, seems to be more significant than the indirect structural matrix T. Therefore we evaluated a new model that emphasize the contribution of the direct structural connections. This model managed to outperform the previous models, achieving

Model	SSE	AIC	BIC
Model 1	85.0444	-178.8344	-176.0011
Model 2	84.4582	-176.2362	-172.4584
Model 3	86.6313	-180.4987	-177.6653
Model 4	85.3328	-177.9468	-174.1691
Model 5	86.6313	-175.5722	-171.7944

Table 2: Performance metrics for the set of single value estimates model

Model	mean α	var α	mean β	var β	mean γ	var γ
Model 1	0.017694	5.8183e-09	-0.10878	1.761e-07	x	x
Model 2	0.020514	9.4917e-09	-0.56207	1.8554e-05	1.1024	9.9962e-05
Model 3	-0.019864	5.506e-08	0.059437	2.8931e-07	x	x
Model 4	0.00093886	7.4477e-08	-0.21169	7.0009e-06	0.51832	3.4875e-05
Model 5	-0.03242	2.0712e-07	-0.14558	2.6495e-07	0.14637	1.1705e-06

Table 3: The quality of the parameter estimates

an SSE of 10.0198, BIC score -179.3634 and AIC score -175.5856.

$$f_{ij} = \alpha_{ij} + \beta_{ij} t_{ij} + \gamma_{ij} s_{ij}^2 \tag{3.6}$$

4 Core Task 3: Advance tasks

To further debunk the complexity of interconnections between the different regions of the brain we explore the structural and functional connectivity graphs, in particular analysing the density of each vertex. Using the structural and functional connectivity density data of each patient, the columns of the 68x68 matrices where summed together to obtain a 1x68 vector. This was done for all 19 patient data, hence these vertex density connections were compiled into a 19x68 matrix, D. Both matrices were more dense, since we are adding all their corresponding edge weights for each vertex. Next, the relationship between the functional and structural connectivity density maps where modelled, independently for each vertex. In other words, investigating whether the structural connectivity density could model the function connectivity density. To do this, I first split the estimated structural connectivity matrix previously computed into training and holdout set, by randomly choosing a patient (or row) to be the holdout set. This was also done for the functional connectivity density data. Then for each vertex (each column) in the structural training data, and ordinary least square method is used, where the $X = \begin{bmatrix} \mathbf{1} & d_j \end{bmatrix}$ where d_j is the column of computed density for vertex j and $\mathbf{1}$ is used as the bias term. Where the model to evaluate this relationship was $f_j = \alpha_j + \beta_j d_j$, where Y is the associated functional density vertex for the given column in the training set. For each vertex the model was tested on a holdout set and the sum of square errors were recorded. The mean sum of errors (MSE) was computed to be 0.002739. Since this MSE is relatively low, this does suggest a strong associations between the modalities.

Furthermore, I looked at repeating the Core Task 2 section but by fitting a single coefficients over all edges, and this time modeled for each patient independently. For this repeat task, the t matrix was computed in the same manner. Subsequently, the 6 models from the previous task were evaluated, now when doing cross validation instead of the training containing 18 patients fMRI data (68x68x18), it will contain a single patient data. In other words, when doing OLS on an individual level, we have that the X matrix will be of dimension (68x68x1, 2) rather than (68x68x18, 2) matrix for the first model. Once the estimated parameters are computed, each patient model is evaluated on a random other patient data. To investigate whether the results generalize well, when using the estimated parameters to compute the functional connectivity of another patient. Table 4 displays the performance metrics for each model. Although we are taking evaluating on every individual patient model for each regression, the average SSE across the 19 different models were recorded for

Model	SSE	AIC	BIC
Model 1	89.083909	-179.414027	-176.580711
Model 2	89.117131	-175.649498	-171.871742
Model 3	90.577479	-178.389100	-175.555783
Model 4	88.286825	-176.616037	-172.838282
Model 5	88.818008	-175.057110	-171.279354
Model 6	130.866563	-155.407717	-151.629961

Table 4: Performance metrics for each lasso model

Model	mean α	var α	mean β	var β	mean γ	var γ
Model 1	0.017776	-0.109657	-0.10878	0.000060	x	x
Model 2	0.020612	0.000003	-0.579480	0.007428	1.146841	0.040837
Model 3	0.017776	0.000002	-0.109657	0.000060	x	x
Model 4	0.020612	0.000003	-0.579480	0.007428	1.146841	0.040837
Model 5	-0.035291	0.000090	-0.147033	0.000080	0.153614	0.000480
Model 6	-0.035291	0.000090	-0.147033	0.000080	0.153614	0.000480

Table 5: The quality of the parameter estimates of lasso model

simplicity. As it is turns out, the performance across the models are generally much lower than when using the other patient data as a general training set. The relatively high SSEs, similar values across the models for each patient and similar parameter mean and variances, further suggests that regardless the patient's structural and functional connections, they are significantly different and hence we should not use this approach to generalise on others.

Due to the nature of how the wiring is formed in the brain, the structural connectivity graph is a sparse matrix. Therefore when dealing with such conditions, using a model based on LASSO would be more suitable. LASSO is a type of linear regression that uses a shrinking parameter, λ. This parameter is used to penalize the loss function when training, to encourage simpler models that have relatively small weights. This effect of shrinking would be done on variables that do not contribute to the overall output. The aim to using this method is to relate each functional connection to a subset of structural connections. This was implemented using a 3-fold cross validation, where for every fold a training set and holdout set were constructed. Then for each fold, I iterated over every functional connection running a lasso regression, using the built-in Matlab function called *lasso()*. This function returns a matrix of row dimension 68x68 and an array of columns for attributed to an array of λ values. Where each column is a column vector of coefficients for each functional connection. In other words the non-zero values in the 68x68 entries of each row are the subset of structural connections. Here, the lowest λ in the array will act closer to an OLS approach, but this array contains an incremental number of λ. For computational efficiency, the coefficient used for computing the predicted functional connection was the column that was positioned at the 70% of the number of lambdas computed. As the largest lambda would have basically all zeros as coefficients and 70% seemed best suited for the number of non-zero coefficient. Then the SSE was computed for each voxel and this was done for 3 folds. The averages of the SSE across all voxels was computed to be 0.07848 over all 3 folds. This MSE is low, and therefore due to the sparse nature of this problem, the lasso approach is a good performing model. It is worth noting that if more

computational power was provided, taking a leave one out for each voxel model and then recording the lambda with the lowest MSE rather than just using an arbitrary lambda position.

References

[1] Jonathan D. Claydon. *Imaging connectivity: MRI and the structural networks of the brain.* Functional neurology vol. 28,3 (2013) 197-203. doi:10.11138/FNeur/2013.28.3.197.

[2] David Miller. "13 - Natural History of Multiple Sclerosis: When Do Axons Degenerate?" In: *Multiple Sclerosis As A Neuronal Disease*. Ed. by Stephen G. Waxman. Burlington: Academic Press, 2005, pp. 185–200. ISBN: 978-0-12-738761-1. DOI: https://doi.org/10.1016/B978-012738761-1/50014-6. URL: https://www.sciencedirect.com/science/article/pii/B9780127387611500146.

[3] B. Sen. *Ranking Regions, Edges and Classifying Tasks in Functional Brain Graphs by Sub-Graph Entropy.* URL: https://doi.org/10.1038/s41598-019-44103-8. Sci Rep 9, 7628 (2019).

[4] Xi Zhang et al. "Gender Differences Are Encoded Differently in the Structure and Function of the Human Brain Revealed by Multimodal MRI". In: *Frontiers in Human Neuroscience* 14 (2020). ISSN: 1662-5161. DOI: 10.3389/fnhum.2020.00244. URL: https://www.frontiersin.org/article/10.3389/fnhum.2020.00244.